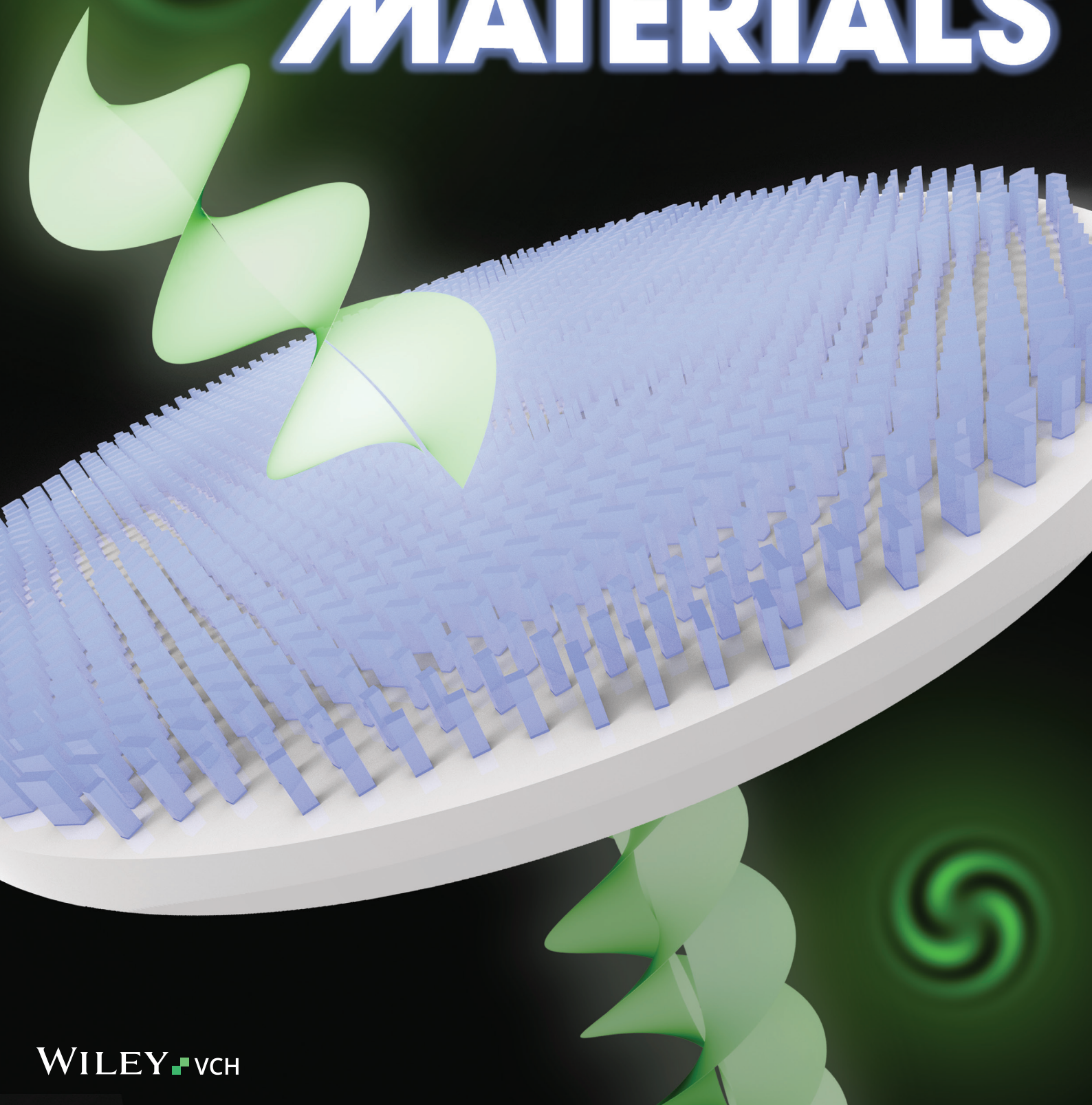


Vol. 12 • No. 31 • November 5 • 2024

[www.advopticalmat.de](http://www.advopticalmat.de)

# ADVANCED OPTICAL MATERIALS



# Directionally Asymmetric in Orbital Angular Momentum Generation Using Single-Layer Dielectric Janus Metasurfaces

Chang-Yi Lin, Jhih-Hao Huang, Huan-Teng Su, Shu-Ming Chang, Yun-Chien Wu, and Yao-Wei Huang\*

Janus metasurfaces, offering versatile light manipulation contingent on incident direction, are explored across microwave to mid-infrared spectra. Nonetheless, prior designs often resort to spatial multiplexing or vertical stacking, entailing complex fabrication. Metallic Janus metasurfaces, owing to material properties, suffer notable Ohmic losses in the visible spectrum. In this study, single-layer TiO<sub>2</sub>-based Janus metasurfaces with arbitrary polarization control is experimentally demonstrated, exhibiting directionally asymmetric functionalities in spin and orbital angular momentum (OAM). A novel Jones matrix formulation tailored for Janus metasurfaces is presented, enabling efficient generation of two asymmetric, high-purity OAM states of vortex beams at wavelength of 532 nm, contingent on incidence direction. This innovation facilitates compact and versatile phase manipulation, encompassing applications such as lasers and optical combiners, thereby expanding its utility across diverse domains.

beams by many methods including spiral plates,<sup>[11]</sup> q-plates,<sup>[12–14]</sup> and J-plates<sup>[15–17]</sup> have been conducted.

Spin-to-orbital angular momentum conversions commonly exhibit directional symmetry (same quantum number for forward and backward directions) or anti-symmetry (opposite sign of quantum number for forward and backward directions), characterized by Pancharatnam-Berry (geometric) phase and propagation phase, respectively. For instance, consider q-plates: counterclockwise rotation of birefringence building blocks along the azimuthal angle remains counterclockwise when observed from opposite directions, yielding the conversion of identical (symmetric) OAM states with the same spin in both directions. In contrast, propagation-phase-based building blocks, for example, spiral

## 1. Introduction

The vortex beam with orbital angular momentum (OAM) is characterized by a helical wavefront with azimuthal phase  $\exp(im\phi)$  where  $m$  is the quantum number that can be any integer and  $\phi$  is the azimuthal angle in the cross section of the beam.<sup>[1–3]</sup> These unique profiles have made significant contribution and found application of quantum information,<sup>[4,5]</sup> optical communication,<sup>[6,7]</sup> microscopy,<sup>[8]</sup> vortex laser technologies,<sup>[9,10]</sup> etc. So far, many studies about producing the optical vortex

plates, alter in thicker and thinner height (or wider and thinner width of nanopillars) along the azimuthal angle when observed from opposite directions, resulting in opposite (anti-symmetric) OAM states. J-plates possess the capability to impart asymmetric OAM states (can be neither symmetric nor anti-symmetric) for the arbitrary two orthogonal spins through a hybrid mechanism involving both geometric and propagation phases.<sup>[9,17]</sup> However, their functionalities are currently confined to one-way transmission. While metallic Janus metasurfaces employing spatial multiplexing have been successfully crafted for microwave applications,<sup>[18–20]</sup> metals commonly encounter challenges such as high absorption and pronounced reflection of electromagnetic radiation across a broad spectrum ranging from visible light to near-infrared and ultraviolet wavelengths, attributable to their inherent optical and electrical characteristics. Additionally, two-layer (vertical stacking) Si-based Janus metasurfaces have been developed in mid-infrared spectra, suffering from complicated fabrication techniques.<sup>[21]</sup> The previously mentioned Janus metasurfaces operate exclusively in either linearly polarized states<sup>[18,19]</sup> or circularly polarized states.<sup>[20,21]</sup> However, there is currently no research addressing the generation of directionally asymmetric OAM from arbitrary spin states.

Here, we demonstrate our Janus metasurfaces that have capability of directionally asymmetric in angular momentum using the single-layer dielectric metasurface operating in the visible. We numerically clarify how the functionalities are for the

C.-Y. Lin, J.-H. Huang, H.-T. Su, S.-M. Chang, Y.-C. Wu, Y.-W. Huang  
Department of Photonics  
College of Electrical and Computer Engineering  
National Yang Ming Chiao Tung University  
Hsinchu 300093, Taiwan  
E-mail: [ywh@nycu.edu.tw](mailto:ywh@nycu.edu.tw)

 The ORCID identification number(s) for the author(s) of this article can be found under <https://doi.org/10.1002/adom.202401335>

© 2024 The Author(s). Advanced Optical Materials published by Wiley-VCH GmbH. This is an open access article under the terms of the [Creative Commons Attribution](https://creativecommons.org/licenses/by/4.0/) License, which permits use, distribution and reproduction in any medium, provided the original work is properly cited.

DOI: 10.1002/adom.202401335

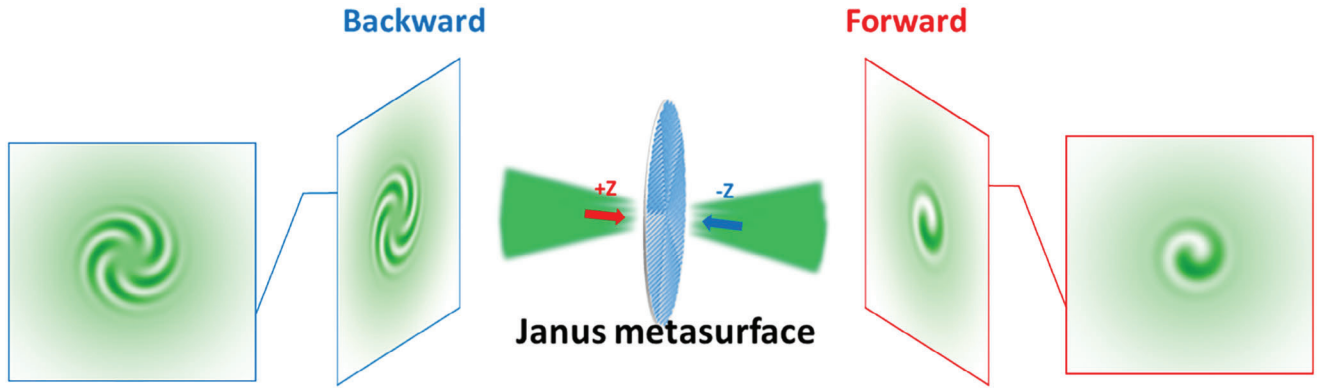


**Figure 1.** Schematic of the Janus metasurface designed to operate at a wavelength of 532 nm. When polarized light is illuminated into the metasurface from different sides, it yields different OAM states. The images of the interference pattern on either side depict the phase of the OAM states of 1 and 5.

forward (+z direction) and backward (-z direction) incidence in their corresponding coordinate system. Distinguished from the previously derived metasurface function in the same direction,<sup>[22,23]</sup> our derivation pertains to the metasurface function enabling distinct OAM for bidirectional light propagation. This kind of Janus metasurface can generate different OAM states depending on the direction of the incident light, which offers the degree of freedom to control the phase. Following the coordinated transformation we propose, high-quality OAM states generated from both sides are achieved by using propagation phase and geometric phase modulation. The schematic of our Janus metasurface (Janus-1) is depicted in **Figure 1**. Vortex beams carrying OAM states of 1 and 5 are illustrated on either side of the Janus metasurface, representing forward and backward incident light with left-hand circular polarization (LCP) in their respective coordinate systems. It is worth noting that the spin state of the incident light can be any arbitrary elliptically polarized state, as demonstrated in our other Janus metasurfaces (Janus-2 and Janus-3).

## 2. Results

### 2.1. Janus Metasurfaces

As well known, the complex transmission of a rectangular meta-atom can be described by the Jones matrix like a conventional linearly birefringence wave plate.<sup>[22,23]</sup> However, there are difference between the local matrix of the metasurface for the forward and backward incidence, which results in the different phase imposing from the meta-atoms as:

$$J = R(-\alpha) \begin{bmatrix} e^{i\varphi_x} & 0 \\ 0 & e^{i\varphi_y} \end{bmatrix} R(\alpha) \quad (1)$$

$$J' = R(-\alpha') \begin{bmatrix} e^{i\varphi_x} & 0 \\ 0 & e^{i\varphi_y} \end{bmatrix} R(\alpha') \quad (2)$$

Here,  $\varphi_x$  and  $\varphi_y$  are the phase shifts as polarized light propagates along  $x$  and  $y$  axes of the meta-atom, the alpha ( $\alpha$  and  $\alpha'$ ) represent the rotation angle defined by their own coordinate systems and the prime sign ( $'$ ) denotes the difference between the

forward and backward coordinate (see Section S1, Supporting Information).

Now, we expect to fulfill a single metasurface that can generate asymmetric functions when the same arbitrary polarized light incidents from the forward and backward direction. Here, we design the metasurface which imparts the OAM states of  $m$  and  $n'$  for the two sides incidence. The element of the global matrix at any position  $(x, y)$  of the metasurface is given by

$$J(x, y) |\lambda\rangle = e^{im\phi(x,y)} |\lambda\rangle^* \quad (3)$$

$$J(x, y) |\lambda'\rangle = e^{in'\phi'(x',y')} |\lambda'\rangle^* \quad (4)$$

Here, the asterisk sign (\*) denotes the complex conjugate of electric field and  $\phi(x, y)$  is the azimuthal angle of the meta-atom on the metasurface. The eigen polarized states  $|\lambda\rangle$  is  $[\cos \chi; \exp(i\delta)\sin \chi]$ , or written in  $|\lambda(\chi, \delta)\rangle$  or  $|\chi, \delta\rangle$ , where  $\chi$  and  $\delta$  are the ellipticity and phase delay of the polarized light. After the coordinated transformation shown in Section S2 (Supporting Information), we can easily derive the Janus metasurface function  $J(x, y)$  by following the two equations above as

$$J(x, y) = \begin{bmatrix} (e^{im\phi(x,y)} + e^{in'\phi'(x',y')}) \cos \chi \sin \chi & e^{-i\delta} (e^{im\phi(x,y)} - e^{in'\phi'(x',y')}) \cos^2 \chi \\ e^{-i\delta} (e^{im\phi(x,y)} - e^{in'\phi'(x',y')}) \sin^2 \chi & e^{-i2\delta} (e^{im\phi(x,y)} + e^{in'\phi'(x',y')}) \cos \chi \sin \chi \end{bmatrix} \quad (5)$$

This matrix is converted to the forward coordinate for simple calculation. A single layer Janus metasurface requires that the global matrix at each position on the metasurface needs to meet the local matrix derived in Equations (1) and (2). The condition requires two off-diagonal elements of the global matrix to be identical.<sup>[24]</sup> With the condition, we find the polarization of the incident light has a physical restriction  $\cos^2 \chi = \sin^2 \chi$  (see Section S2, Supporting Information). This completion clarifies that the eigenpolarizations of our Janus metasurface must satisfy  $\chi = \pi/4$ , while  $\delta$  can be any real number as the degree of freedom of the design. However, the restriction makes the Janus metasurface only work for a few specific polarizations, which significantly reduces the application range of it. To break this limitation, we further adopt the other degree of freedom in designing Janus metasurfaces by taking the rotation of the entire global matrix into consideration. As the global matrix rotates with an angle of

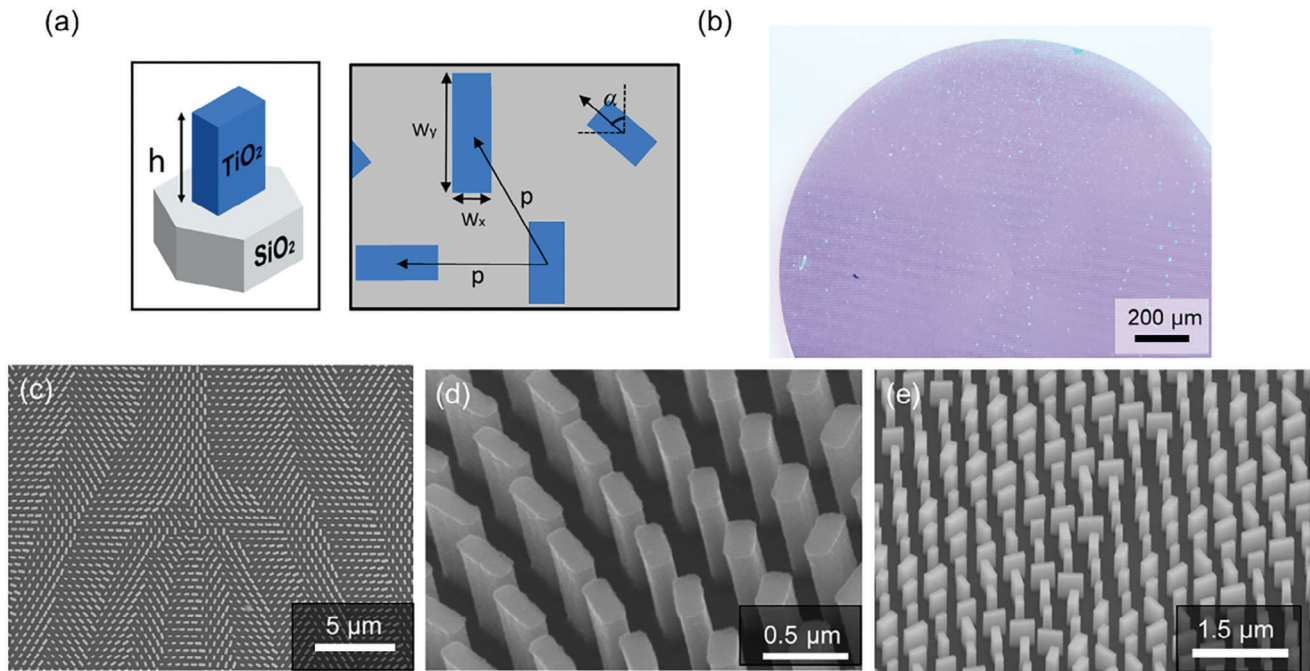


**Figure 2.** Design and fabricated Janus metasurfaces. a) Schematic of 600-nm-height of rectangular  $\text{TiO}_2$  meta-atom on fused silica substrate with 500-nm-period hexagonal lattice (left). Arrangement of meta-atoms with geometric parameters: widths ( $W_x$ ,  $W_y$ ), period ( $p$ ), and rotation angle ( $\alpha$ ) (right). b) Optical microscope image of Janus-2. c–e) Scanning electron microscope images of the central parts of Janus-1 (c), Janus-2 (d), and Janus-3 (e).

$\beta$ , the eigenpolarization also follows the conversion, leading to a new polarized state. The process can be derived as

$$J |\lambda\rangle = J \left| \frac{\pi}{4}, \delta \right\rangle = JR(-\beta) R(\beta) \left| \frac{\pi}{4}, \delta \right\rangle = J_\beta |\chi_d, \delta_d\rangle \quad (6)$$

where  $|\pi/4, \delta\rangle$  denotes the original polarization with the restriction  $\chi = \pi/4$ ,  $R(\beta)$  is the rotation matrix,  $J_\beta = JR(-\beta)$  is the global matrix after rotation, and  $|\chi_d, \delta_d\rangle = R(\beta)|\pi/4, \delta\rangle$  is the target polarization of design in which  $\chi_d$  and  $\delta_d$  are for an arbitrary state. The related derivation is depicted in Section S3 (Supporting Information). Therefore, the arbitrary polarized state can successfully demonstrate different desired OAM states from forward and backward incidence.

## 2.2. Fabrication

In our design, we establish rectangular  $\text{TiO}_2$  meta-atoms with a fixed height ( $h$ ) of 600 nm, arranged in a hexagonal lattice pattern on a fused silica substrate with a period ( $p$ ) of 500 nm for each lattice arrangement, as illustrated in Figure 2a. The  $\varphi_x$ ,  $\varphi_y$ , and local rotation angle ( $\alpha$ ) of each meta-atom must satisfy the global matrix shown in Equation (5) and are obtained using the method described in the literature.<sup>[15,23]</sup> Additionally, a global rotation angle ( $\beta$ ) is applied to each meta-atom on Janus-3. The width ( $W_x$ ,  $W_y$ ) of each meta-atom is then designed to impart the desired phase delay at a wavelength of 532 nm obtained by our phase-to-width lookup table (see Section S4, Supporting Information).

To fulfill the asymmetric vortex beam generation from a single dielectric Janus metasurfaces by following the theory we derive,

we design and fabricate 3 Janus metasurfaces for circular and elliptical polarized light: Janus-1 with circular eigenpolarization  $|\pi/4, \pi/2\rangle$ , the forward and backward imposing OAM states are  $[m, n] = [+1, +5]$ . Janus-2 and Janus-3 are with different elliptical polarized states and impart different OAM states, which are listed in Table 1. We note that Janus-2 has  $\chi = \pi/4$ , which makes its two off-diagonal elements of the global matrix identical and satisfies Equation (5). In contrast, Janus-3 has  $\chi = \pi/6$ , providing an additional degree of freedom in the global rotation of the sample (Equation (6)), thereby breaking the design limitation imposed by Equation (5). The fabrication process involves electron-beam lithography, atomic layer deposition, and etching techniques. All our Janus metasurfaces were fabricated following the procedures outlined in reference. Figure 2c–e represents scanning electron microscope (SEM) images of three fabricated Janus metasurfaces.

We note that Janus-1 and Janus-2 have an additionally grating phase with a deflection polar angle ( $\theta_d$ ) of  $5^\circ$  and deflection azimuthal angle ( $\phi_d$ ) of  $0^\circ$ , in the spherical coordinate system. For Janus-3, We add a more complex grating phase of deflection polar and azimuthal angles ( $\theta_d, \phi_d$ ) of  $(25.1^\circ, 101.8^\circ)$ , although these values can be arbitrary. The additional grating phase

**Table 1.** Three Janus metasurface designs.

	$ \lambda(\chi, \delta)\rangle$	Forward OAM state	Backward OAM state
Janus-1	$ \frac{\pi}{4}, \frac{\pi}{2}\rangle$	1	5
Janus-2	$ \frac{\pi}{4}, \frac{\pi}{4}\rangle$	2	-3
Janus-3	$ \frac{\pi}{6}, \frac{\pi}{3}\rangle$	2	-4

helps to obtain a purer OAM state of the vortex beam at the 1st order diffraction, eliminating the polarization-unconverted term at the 0th order, as demonstrated in the literature.<sup>[15,16]</sup> The detail replacement of Equations (3), (4), and (5) regarding to additional grating phase on Janus 1–3 is written in Section S5 (Supporting Information). And the method to generate the layout of Janus metasurfaces is shown in Section S6 (Supporting Information).

### 2.3. OAM Characteristics

To illustrate our Janus metasurfaces, we constructed an experimental setup for measurement (see Section S7, Supporting Information). We configure the laser with a wavelength of 532 nm as the incident light. The polarizations of incidence include various corresponding to Janus 1–3, as detailed in Table 1. These configurations account for both forward and backward propagation through the metasurfaces. Experimental results as well as simulation results of three Janus metasurfaces are illustrated in Figure 3. The measured intensity profiles in Figure 3a feature a distinctive doughnut-shape pattern where size of the central hole is determined by their OAM states. To visualize the phase of these vortex beams, we interfere the vortex beams with a Gaussian beam under a Mach-Zehnder interferometer setup (see Section S7, Supporting Information) and results are shown in Figure 3b. One can well see clear fringe number and rotation direction of Janus 1–3 corresponding to their designed OAM quantum numbers. In addition, the simulated phase profiles are obtained approximately one wavelength away from the meta-atoms through finite-difference time-domain (FDTD) simulation, as depicted in Figure 3c. These phase profiles exhibit  $m$ -fold or  $n$ -fold  $2\pi$  azimuthal angle variations with clockwise or counter-clockwise rotation corresponding to different incident directions and designed OAM quantum numbers. This indicates that the same quantum numbers are obtained from the experimental results shown in Figure 3b. We experimentally impart asymmetric OAM states from Janus metasurfaces from the forward and backward illumination with arbitrary polarizations, as we design.

### 2.4. Polarization Characteristics

In the following analysis, we investigate the polarization conversion characteristics of the metasurfaces. The Stoke parameters of the output polarizations  $\lambda(\chi, \delta)$  through Janus 1–3 from forward and backward illumination are measured. Figure 4 illustrates the Stoke parameters of theoretical (blue), simulated (red), and measured (yellow) output polarizations for forward and backward incidence.

For simulated values of Stoke parameters, we obtained the electric field components along the  $x$ - and  $y$ -directions ( $E_x, E_y$ ) at the donut-shape intensity profiles of the vortex beams from the full-wave FDTD simulation. Then, the Jones vector  $|\chi, \delta\rangle = [\cos \chi; \exp(i\delta)\sin \chi]$  was used to calculate the Stoke parameters of the simulated values using the theoretical formula. The theoretical formula for S1, S2, and S3 are written as:

$$S1 = \cos^2 \chi - \sin^2 \chi \quad (7)$$

$$S2 = 2 \cos \delta \cos \chi \sin \chi \quad (8)$$

$$S3 = 2 \sin \delta \cos \chi \sin \chi \quad (9)$$

For Janus-1, the theoretical output spin states are right circularly polarized (RCP) for forward and backward condition, showing no difference in optical power for any orthogonal linear polarizations, resulting in values of  $\sim 0$  at S1 and S2 and value of  $\sim -1$  at S3. For Janus-2, the theoretical output spin states are  $|\pi/4, -\pi/4\rangle$  and  $|\pi/4, -\pi/4\rangle'$ . The intensity difference between the horizontal and vertical directions is zero but has the phase delay of  $-\pi/4$ , leading to value on S1  $\sim 0$ , while S2 and S3 have theoretical values of 0.707 and  $-0.707$  respectively. Janus-3, corresponding to an arbitrary elliptical polarized state of  $|\chi, \delta\rangle = |\pi/6, \pi/3\rangle$ , contributes theoretical values of 0.500 on S1, 0.433 on S2, and  $-0.750$  on S3.

For experimental values of Stoke parameters, we utilized a set of linear polarizer and quarter wave plate to analyze the output polarization states. These polarization states were projected onto 6 polarization states:  $|x\rangle, |y\rangle, |45^\circ\rangle, |-45^\circ\rangle, |L\rangle, |R\rangle$ . We measured their power ( $P$ ) using a power meter. The Stoke parameters ( $S$ ) can be calculated from the 6 measured values, and transformation is written as:<sup>[16]</sup>

$$P = \begin{bmatrix} P_x \\ P_y \\ P_{45^\circ} \\ P_{-45^\circ} \\ P_L \\ P_R \end{bmatrix} = \begin{bmatrix} 1 & 1 & 0 & 0 \\ 1 & -1 & 0 & 0 \\ 1 & 0 & 1 & 0 \\ 1 & 0 & -1 & 0 \\ 1 & 0 & 0 & 1 \\ 1 & 0 & 0 & -1 \end{bmatrix} \begin{bmatrix} S0 \\ S1 \\ S2 \\ S3 \end{bmatrix} = AS \quad (10)$$

$$S = (A^T A)^{-1} A^T P \quad (11)$$

Additionally, the theoretical output spin states of Janus-3 are  $|\pi/6, -\pi/3\rangle$  and  $|\pi/3, -\pi/3\rangle'$  due to a rotation of  $\beta = -24.6^\circ$  on sample (see Section S3, Supporting Information), resulting in a different set of theoretical, simulated, and measured Stocks parameters. As experimental results shown in Figure 4, Janus 1–3 demonstrate good performance on the polarization conversion, which confirms our Janus metasurfaces operate effectively under arbitrary polarizations (see Section S8, Supporting Information for detail values of Stocks parameters). We observe that the more complex polarized states and diffraction angles of incidence for Janus-3 indeed heighten the challenge in characterizing polarization characteristics, leading to greater disparities between experimental and theoretical Stock parameters compared to Janus-1 and Janus-2.

## 3. Discussion and Conclusion

Previous demonstrations of Janus metasurfaces in the microwave region, particularly for applications such as lenses and holograms, relied on spatial multiplexing.<sup>[18–20]</sup> This approach required the combination of two types of meta-atoms arranged in an interleaved form, operating for each direction. To achieve polarization conversion in each meta-atom, the inclusion of three metallic layers is necessary. Another approach to achieve asymmetry functionalities was through the use of multi-layer metasurfaces, exemplified by the logic gate focusing demonstrated by

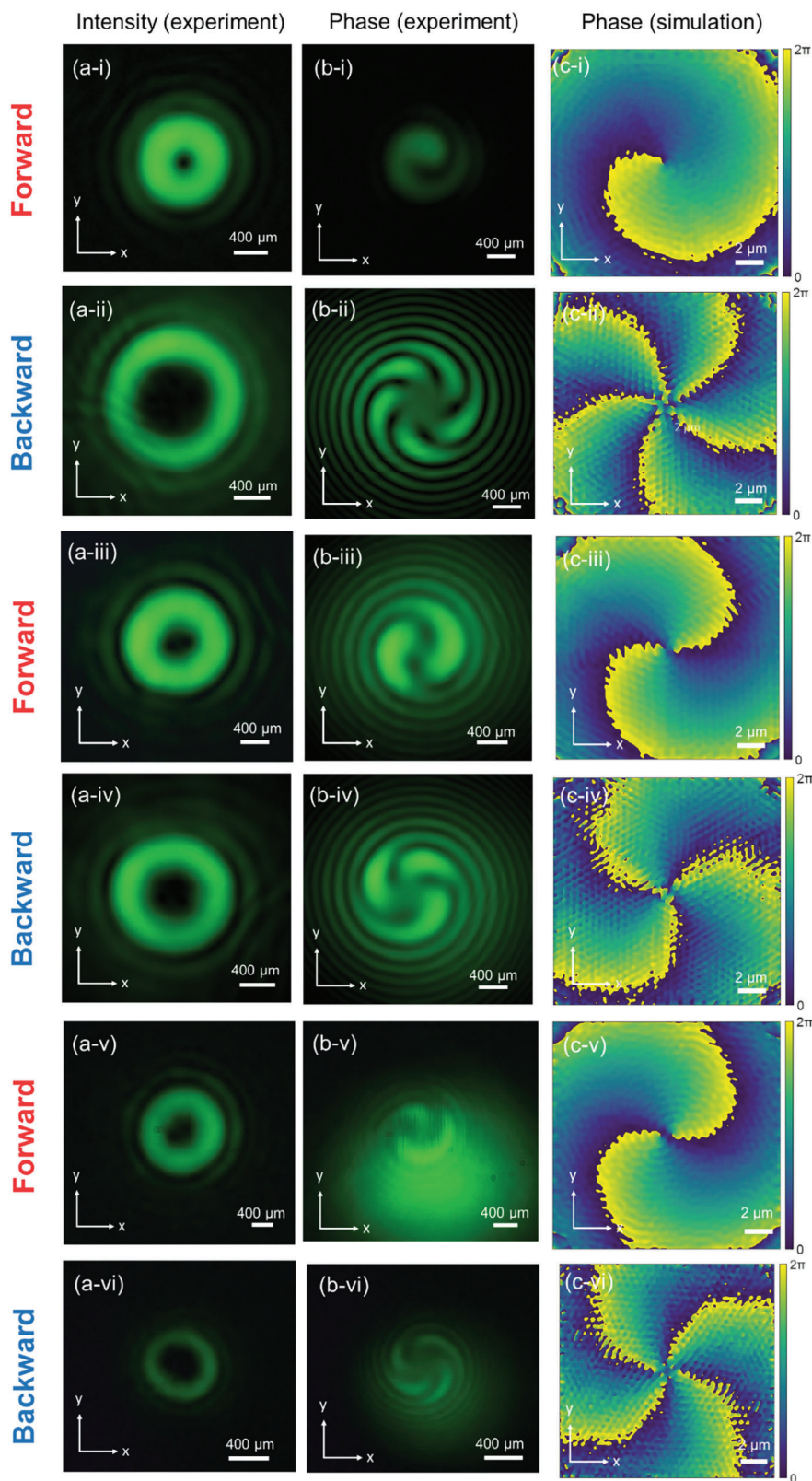


**Figure 3.** The experimental and simulated results of three Janus metasurfaces for the forward and backward incidence. a) Experimental intensity distribution of the output states. b) Experimental interference fringes of the output states. c) Simulated phase profile of the output states. Results from (i) to (vi) correspond to Janus-1 forward and backward incidence, Janus-2 forward and backward incidence, and Janus-3 forward and backward incidence.

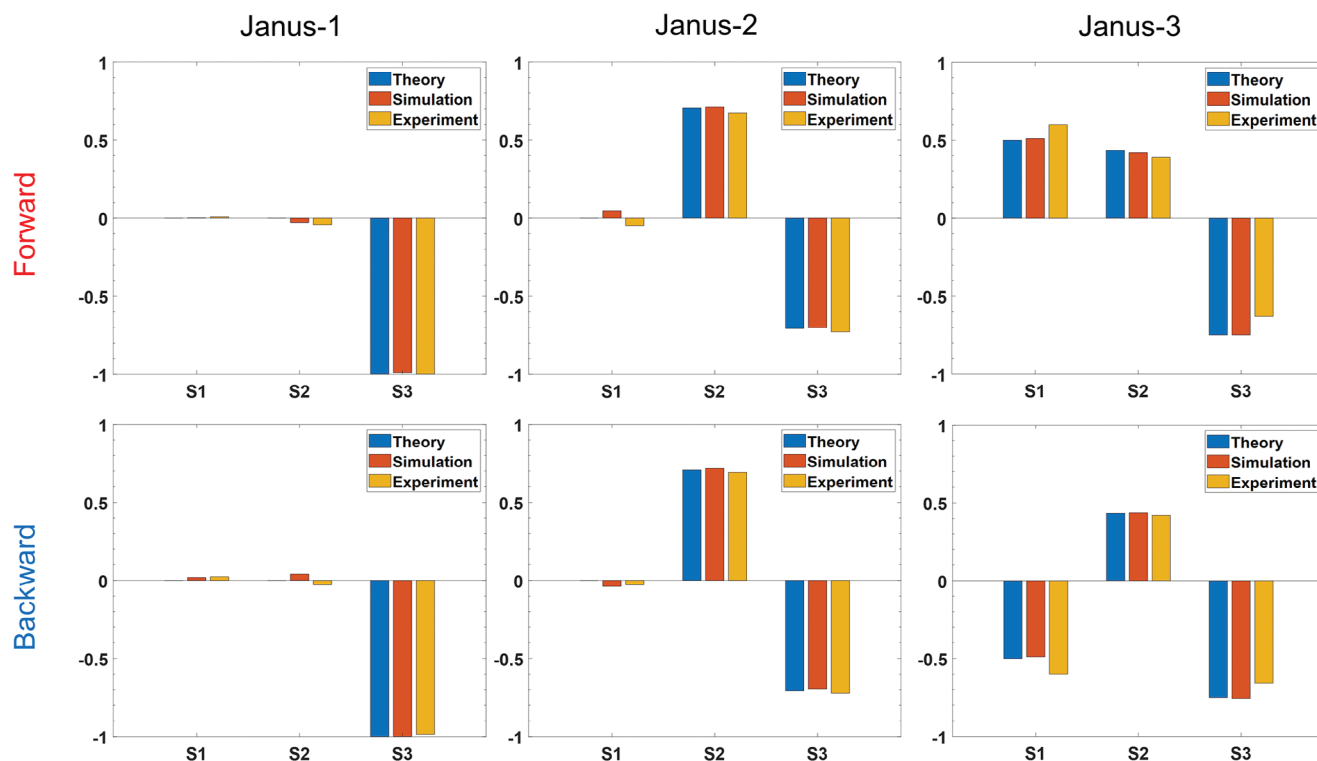


**Figure 4.** The theoretical (blue), simulated (red), and measured (yellow) Stoke parameters of output polarizations from Janus 1, 2, and 3 for forward and backward incidence. The values of S1, S2, and S3 are represented by bar charts. For more detailed values of the Stokes parameters, please refer to Section S8 (Supporting Information).

Si-based doublet metalens operating in the mid-infrared range.<sup>[21]</sup> In contrast, our approach with single-layer dielectric Janus metasurfaces offers a streamlined alternative, effectively achieving asymmetric OAM states across arbitrary spin configurations in the visible region.

There is still a constraint in our Janus metasurfaces regarding the generation of high-order OAM states. Since our design does not take amplitude modulation into account, this method achieves a qualitatively purer OAM state only for low OAM quantum numbers. Both the measured interference fringe (Figure 3b) and the simulated phase distribution (Figure 3c) clearly provide a qualitative check of our OAM state. For higher OAM modes or spatial nanoscale generation, both amplitude and phase modulation on metasurfaces need to be considered, and a further quantitative check of OAM states is required.<sup>[9,17,25,26]</sup>

In summary, by the coordinated transformation, we clarify the relation of the local and global matrix of the Janus metasurfaces for the forward and backward conditions. We utilized degrees of freedom such as global rotation, local rotation, and the width of meta-atoms to achieve any polarization state. Specifically, the width of the meta-atoms achieves the propagation phase, local rotation achieves the geometric phase, and global rotation achieves elliptical polarizations where  $\chi$  is not limited to  $\pm\pi/4$ . Following our design, we successfully create single layer TiO<sub>2</sub>-based Janus metasurfaces that has the capability of generating the asymmetry OAM states according to their direction of incidence. High performance and good polarization conversion of the vortex beams for the two sides incidence generated by the Janus metasurfaces

are theoretically and experimentally demonstrated. The intensity profiles show the featured donut-shape distribution of vortex beams with the pure singularity and lobes of the interference pattern correspond to our designed OAM states and simulation results. Besides, the Stoke parameters of output polarizations from the experiment nearly match with the theoretical and simulated values. These excited features lead us firmly believe that our design for the Janus metasurface will continue to play a significant role in the ongoing development of meta-optics, unlocking further functionalities and applications in such optical combiners,<sup>[27]</sup> intra-cavity mode modulation in lasers,<sup>[9]</sup> multifunctionalities for receiver and transceiver,<sup>[28]</sup> space-time coupling,<sup>[29–31]</sup> etc.

## Supporting Information

Supporting Information is available from the Wiley Online Library or from the author.

## Acknowledgements

This work was supported by the National Science and Technology Council in Taiwan (Grant Nos. 110-2112-M-A49-034-MY3 and 113-2112-M-A49-025). The authors also acknowledge support from the Ministry of Education in Taiwan under the Yushan Young Scholar Program and the Higher Education Sprout Project of the National Yang Ming Chiao Tung University. This work was performed in part at the Nano Facility Center (NFC) in NYCU, Center for Nano Science and Technology (CNST) in NYCU, and

the Taiwan Semiconductor Research Institute (TSRI). The authors also acknowledge Dr. Zhujun Shi for technical discussion.

## Conflict of Interest

The authors declare no conflict of interest.

## Author Contributions

Y.-W.H. initiated the study and contributed required materials and analysis tools. C.-Y.L. and J.-H.H. performed the numerical calculation and simulation. C.-Y.L., J.-H.H., H.-T.S., S.-M.C., and Y.-C.W. fabricated metasurface samples. C.-Y.L. and J.-H.H. performed the optical experiments. C.-Y.L., J.-H.H., and Y.-W.H. analyzed experimental data. C.-Y.L. and Y.-W.H. wrote the manuscript. All authors discussed the results and commented on the manuscript.

## Data Availability Statement

The data that support the findings of this study are available from the corresponding author upon reasonable request.

## Keywords

arbitrary polarization, directional asymmetry, Janus metasurfaces, orbital angular momentum, vortex beam

Received: May 16, 2024

Revised: July 27, 2024

Published online: August 29, 2024

- [1] L. Allen, M. W. Beijersbergen, R. J. C. Spreeuw, J. P. Woerdman, *Phys. Rev. A* **1992**, 45, 8185.
- [2] M. J. Padgett, *Opt. Express* **2017**, 25, 11265.
- [3] Y. Shen, X. Wang, Z. Xie, C. Min, X. Fu, Q. Liu, M. Gong, X. Yuan, *Light-Sci. Appl.* **2019**, 8, 90.
- [4] M. Wang, L. Chen, D.-Y. Choi, S. Huang, Q. Wang, C. Tu, H. Cheng, J. Tian, Y. Li, S. Chen, H.-T. Wang, *Nano Lett.* **2023**, 23, 3921.
- [5] T. Stav, A. Faerman, E. Maguid, D. Oren, V. Kleiner, E. Hasman, M. Segev, *Science* **2018**, 361, 1101.
- [6] Y. Yan, G. Xie, M. P. J. Lavery, H. Huang, N. Ahmed, C. Bao, Y. Ren, Y. Cao, L. Li, Z. Zhao, A. F. Molisch, M. Tur, M. J. Padgett, A. E. Willner, *Nat. Commun.* **2014**, 5, 4876.
- [7] Q. Mai, C. Wang, X. Wang, S. Cheng, M. Cheng, Y. He, J. Xiao, H. Ye, D. Fan, Y. Li, S. Chen, *J. Lightwave Technol.* **2021**, 39, 6159.
- [8] T. A. Klar, S. W. Hell, *Opt. Lett.* **1999**, 24, 954.
- [9] H. Sroor, Y.-W. Huang, B. Sephton, D. Naidoo, A. Vallés, V. Ginis, C.-W. Qiu, A. Ambrosio, F. Capasso, A. Forbes, *Nat. Photonics* **2020**, 14, 498.
- [10] Z. Qiao, Z. Yuan, S. Zhu, C. Gong, Y. Liao, X. Gong, M. Kim, D. Zhang, Y.-C. Chen, *Optica* **2023**, 10, 846.
- [11] M. W. Beijersbergen, R. P. C. Coerwinkel, M. Kristensen, J. P. Woerdman, *Opt. Commun.* **1994**, 112, 321.
- [12] G. Biener, A. Niv, V. Kleiner, E. Hasman, *Opt. Lett.* **2002**, 27, 1875.
- [13] L. Marrucci, C. Manzo, D. Paparo, *Phys. Rev. Lett.* **2006**, 96, 163905.
- [14] R. C. Devlin, A. Ambrosio, D. Wintz, S. L. Oscurato, A. Y. Zhu, M. Khorasaninejad, J. Oh, P. Maddalena, F. Capasso, *Opt. Express* **2017**, 25, 377.
- [15] R. C. Devlin, A. Ambrosio, N. A. Rubin, J. P. B. Mueller, F. Capasso, *Science* **2017**, 358, 896.
- [16] Y.-W. Huang, N. A. Rubin, A. Ambrosio, Z. Shi, R. C. Devlin, C.-W. Qiu, F. Capasso, *Opt. Express* **2019**, 27, 7469.
- [17] B. Sephton, Y.-W. Huang, A. Ambrosio, C.-W. Qiu, A. Vallés, T. Omatsu, F. Capasso, A. Forbes, *J. Nanophotonics* **2020**, 14, 1.
- [18] K. Chen, G. Ding, G. Hu, Z. Jin, J. Zhao, Y. Feng, T. Jiang, A. Alù, C.-W. Qiu, *Adv. Mater.* **2020**, 32, 1906352.
- [19] Z. Tang, L. Li, H. Zhang, J. Yang, J. Hu, X. Lu, Y. Hu, S. Qi, K. Liu, M. Tian, J. Jin, Z. Zhang, H. Lin, Y. Huang, *Mater. Des.* **2022**, 223, 111264.
- [20] W. Yang, K. Chen, S. Dong, S. Wang, K. Qu, T. Jiang, J. Zhao, Y. Feng, *ACS Appl. Mater. Interfaces* **2023**, 15, 27380.
- [21] Y. Huang, T. Xiao, S. Chen, Z. Xie, J. Zheng, J. Zhu, Y. Su, W. Chen, K. Liu, M. Tang, P. Müller-Buschbaum, L. Li, *Opto-Electron. Adv.* **2023**, 6, 220073.
- [22] A. Arbabi, Y. Horie, M. Bagheri, A. Faraon, *Nat. Nanotechnol.* **2015**, 10, 937.
- [23] J. P. Balthasar Mueller, N. A. Rubin, R. C. Devlin, B. Groever, F. Capasso, *Phys. Rev. Lett.* **2017**, 118, 113901.
- [24] C. Menzel, C. Rockstuhl, F. Lederer, *Phys. Rev. A* **2010**, 82, 053811.
- [25] Q. Chen, G. Qu, J. Yin, Y. Wang, Z. Ji, W. Yang, Y. Wang, Z. Yin, Q. Song, Y. Kivshar, S. Xiao, *Nat. Nanotechnol.* **2024**, 19, 1000.
- [26] M. de Oliveira, M. Piccardo, S. Eslami, V. Aglieri, A. Toma, A. Ambrosio, *ACS Photonics* **2023**, 10, 290.
- [27] M. L. Brongersma, *SPIE* **2019**, 11080, 110800R.
- [28] X. G. Zhang, Y. L. Sun, B. Zhu, W. X. Jiang, Q. Yu, H. W. Tian, C.-W. Qiu, Z. Zhang, T. J. Cui, *Light-Sci. Appl.* **2022**, 11, 126.
- [29] H. B. Sedeh, M. M. Salary, H. Mosallaei, *Nanophotonics* **2020**, 9, 2957.
- [30] M. Piccardo, M. de Oliveira, V. R. Policht, M. Russo, B. Ardini, M. Corti, G. Valentini, J. Vieira, C. Manzoni, G. Cerullo, A. Ambrosio, *Nat. Photonics* **2023**, 17, 822.
- [31] B. Chen, Y. Zhou, Y. Liu, C. Ye, Q. Cao, P. Huang, C. Kim, Y. Zheng, L. K. Oxenløwe, K. Yvind, J. Li, J. Li, Y. Zhang, C. Dong, S. Fu, Q. Zhan, X. Wang, M. Pu, J. Liu, *Nat. Photonics* **2024**, 18, 625.